Archives of Biochemistry and Biophysics 736 (2023) 109517

Contents lists available at ScienceDirect

Archives of Biochemistry and Biophysics

journal homepage: www.elsevier.com/locate/yabbi

Mammalian dihydropyrimidine dehydrogenase: Added mechanistic details from transient-state analysis of charge transfer complexes

Madison M. Smith, Dariush C. Forouzesh, Nicholas E. Kaley, Dali Liu, Graham R. Moran *

Department of Chemistry and Biochemistry, 1068 W Sheridan Rd, Loyola University Chicago, Chicago, IL, 60660, USA

ARTICLE INFO

Keywords:
Pyrimidine
Flavin
Iron-sulfur center
Oxidoreductase
Transient-state kinetics
Charge-transfer absorption

ABSTRACT

Dihydropyrimidine dehydrogenase (DPD) is a flavin dependent enzyme that catalyzes the reduction of the 5,6-vinylic bond of pyrimidines uracil and thymine with electrons from NADPH. DPD has two active sites that are separated by ~60 Å. At one site NADPH binds adjacent to an FAD cofactor and at the other pyrimidine binds proximal to an FMN. Four Fe_4S_4 centers span the distance between these active sites. It has recently been established that the enzyme undergoes reductive activation prior to reducing the pyrimidine. In this initial process NADPH is oxidized at the FAD site and electrons are transmitted to the FMN via the Fe_4S_4 centers to yield the active state with a cofactor set of FAD•4(Fe_4S_4)•$FMNH_2$. The catalytic chemistry of DPD can be studied in transient-state by observation of either NADPH consumption or charge transfer absorption associated with complexation of NADPH adjacent to the FAD. Here we have utilized both sets of absorption transitions to find evidence for specific additional aspects of the DPD mechanism. Competition for binding with $NADP^+$ indicates that the two charge transfer species observed in activation/single turnover reactions arise from NADPH populating the FAD site before and after reductive activation. An additional charge transfer species is observed to accumulate at longer times when high NADPH concentrations are mixed with the enzyme•pyrimidine complex and this data can be modelled based on asymmetry in the homodimer. It was also shown that, like pyrimidines, dihydropyrimidines induce rapid reductive activation indicating that the reduced pyrimidine formed in turnover can stimulate the reinstatement of the active state of the enzyme. Investigation of the reverse reaction revealed that dihydropyrimidines alone can reductively activate the enzyme, albeit inefficiently. In the presence of dihydropyrimidine and $NADP^+$ DPD will form NADPH but apparently without measurable reductive activation. Pyrimidines that have 5-substituent halogens were utilized to probe both reductive activation and turnover. The linearity of the Hammett plot based on the rate of hydride transfer to the pyrimidine establishes that, at least to the radius of an iodo-group, the 5-substituent volume does not have influence on the observed kinetics of pyrimidine reduction.

1. Introduction

Dihydropyrimidine dehydrogenase (DPD) catalyzes the first and rate-limiting step of the three transformations that comprise pyrimidine catabolism [1–10]. DPD is a flavin-dependent oxidoreductase that reduces the 5,6-vinylic bond of uracil or thymine with electrons from NADPH (Fig. 1).

The enzyme is a functional homodimer in which each subunit has 1025 amino acid residues and forms two separate substrate binding sites that each have a non-covalently bound flavin cofactor. The FAD containing site binds NADPH and is located 56 Å from the FMN containing site where pyrimidines associate [1,11]. Between these two sites there is an electron conduit comprised of four Fe_4S_4 centers, two from each subunit in a domain V swapped arrangement [11]. Though the Fe_4S_4 centers span the two active sites, they have not yet been observed to reduce during normal catalysis and so are assumed to rapidly transmit electrons from the NADPH•FAD site to the FMN•pyrimidine site [12]. The complexity of the cofactor set belies the simplicity of the chemistry

Abbreviations: DPD, Dihydropyrimidine dehydrogenase; KPi, Dipotassium hydrogen phosphate; EDTA, ethylenediamine-tetraacetic acid; NADP, nicotinamide adenine dinucleotide phosphate; LB, lysogeny broth; 5ClU, 5-chlorouracil; HEPES buffer, 4-(2-hydroxyethyl)-1-piperazineethanesulfonic acid; DTT, dithiothreitol; 5FU, 5-fluorouracil; DHU, 5,6-Dihydrouracil; DHT, 5,6-dihydro-5-methyluracil; 5IU, 5-iodouracil; 5BrU, 5-bromouracil.

* Corresponding author.
E-mail address: gmoran3@luc.edu (G.R. Moran).

https://doi.org/10.1016/j.abb.2023.109517
Received 21 November 2022; Received in revised form 3 January 2023; Accepted 6 January 2023
Available online 18 January 2023
0003-9861/

catalyzed. Indeed, numerous flavin-dependent dehydrogenases accomplish, from a redox standpoint, the same chemistry while having a single active site with a single flavin and a much smaller protein scaffold [13–16].

With examination of the DPD structure, it is tempting to imagine that it functions by transferring two electrons from NADPH to the pyrimidine by transiently reducing each of the intervening cofactors in series. However, it has been shown that the active form of DPD is two-electron reduced and that these electrons reside on the FMN to give the cofactor set: FAD•4(Fe_4S_4)•$FMNH_2$ [9,17] (Scheme 1). When isolated in the presence of dioxygen DPD is oxidized (FAD•4(Fe_4S_4)•FMN) and will rapidly take up two electrons in the presence of NADPH and pyrimidine. During this reductive activation the pyrimidine acts as an effector, as its presence is required to stimulate the rate of NADPH oxidation and subsequent FMN reduction, but the pyrimidine is not reduced during this process.

Only when a second molecule of NADPH binds are electrons passed to the pyrimidine and the second molecule of NADPH is oxidized, not to reduce the pyrimidine but to reinstate the FAD•4(Fe_4S_4)•$FMNH_2$ oxidation state that, from an observational standpoint, appears to happen concomitant with the considerably slower rate of pyrimidine reduction [9]. Under anaerobic conditions and in the absence of NADPH, the activated enzyme does not reoxidize to the FAD•4(Fe_4S_4)• FMN state even in the presence of excess oxidant pyrimidine substrate, suggesting that crosstalk between the two active sites is required for catalysis. This is a highly unusual reaction sequence and the first example of a flavin-dependent dehydrogenase in which the oxidative half-reaction occurs prior to the reductive half-reaction [17]. Additionally, DPD has demonstrated characteristics that are indicative of half-of-sites reactivity. With equimolar NADPH and enzyme in the presence of saturating pyrimidine, half of the available NADPH is oxidized during initial reductive activation, and the remaining NADPH is then consumed, only at the activated subunits, with a rate that is assumed to be contingent on pyrimidine reduction. The steady-state turnover number, however, closely matches the observed rate constant for pyrimidine reduction and so there is no question that both subunits are active [9].

The characterization of this unique reaction sequence has resulted in a series of outstanding mechanistic questions. This study will focus on the examination of net single turnover reactions with the use of a variant form of DPD in which the FMN active site residue cysteine 671 is mutated to a serine. The term net single turnover is used as the dissociation constant for the NADPH•FAD•4(Fe_4S_4)•FMN complex is not known and so NADPH cannot be said to be saturated with the enzyme. Cys671 has been previously identified to be the general acid that resides on a mobile loop that positionally controls access to the FMN active site and the transmittance of electrons from the $FMNH_2$ to the pyrimidine [2,3,9,18]. This mobile element shifts between an inward and an outward position with crosslinking and structural data indicate that the inward position is more prominent when the enzyme is in the reductively activated state [9,18]. Using systematic perturbation of weak charge transfer absorption, we show evidence for asymmetry in the DPD dimer, the role of effectors that stimulate reductive (re)activation, evidence for dihydropyrimidines as reducing substrates, and the influence of substituent volume at the 5-position of the pyrimidine in the pyrimidine reduction hydride transfer reaction. Collectively these observations provide improved characterization and description for numerous aspects of both the activation and catalytic chemistry of DPD.

2. Materials and methods

2.1. Materials and quantitation

Dipotassium hydrogen phosphate (KPi), ethylenediamine-tetraacetic acid (EDTA), nicotinamide adenine dinucleotide phosphate ($NADP^+$), ammonium sulfate, the Miller formulation of lysogeny broth (LB) powder, 5-chlorouracil (5ClU), glycerol, sodium citrate, and 4-(2-hydroxyethyl)-1-piperazineethanesulfonic acid (HEPES) buffer were purchased from Fisher Scientific. Reduced nicotinamide adenine dinucleotide phosphate (NADPH) and dithiothreitol (DTT) were from RPI Research Products. Competent BL21 (DE3) cells were obtained from New England Biolabs. The sodium salt of ampicillin and dextrose powder were obtained from Spectrum Chemical. Uracil, 5-methyluracil (thymine), 5-fluorouracil (5FU), and dithionite were obtained from Acros organics. 5,6-Dihydrouracil (DHU), 5,6-dihydro-5-methyluracil (R,S) (DHT), 5-bromouracil (5BrU), and PEG 6000 were acquired from Alfa Aesar. PEG 400 was obtained from Hampton Research. Glucose oxidase and 5-iodouracil (5IU) were obtained from Millipore Sigma.

The concentrations of each 5-halopyrimidine were defined by mass. The concentrations of the following substrates and products were determined spectrophotometrically using the following extinction coefficients: NADPH; ε_{340} = 6220 $M^{-1}cm^{-1}$, $NADP^+$; ε_{260} = 17 800 $M^{-1}cm^{-1}$, uracil; ε_{260} = 8200 $M^{-1}cm^{-1}$, thymine; ε_{264} = 7860 $M^{-1}cm^{-1}$, DHU; $\varepsilon_{225} = 1280\ M^{-1}cm^{-1}$, DHT; $\varepsilon_{225} = 1670\ M^{-1}cm^{-1}$. The extinction coefficient used to quantify DPD was $\varepsilon_{426} = 75\ 000\ M^{-1}cm^{-1}$ [19].

2.2. Expression and purification of DPD

Recombinant porcine DPD C671S was expressed and purified and stored as described previously [19]. The C671S variant has been characterized and demonstrates slower rates of reductive activation and pyrimidine reduction than are observed for the wild type enzyme [17]. Prior to experiments DPD with DTT (~2 mM in storage) was thawed and diluted into the required buffer to bring the DTT concentration to a negligible level. Exchanges were carried out using repeated steps of

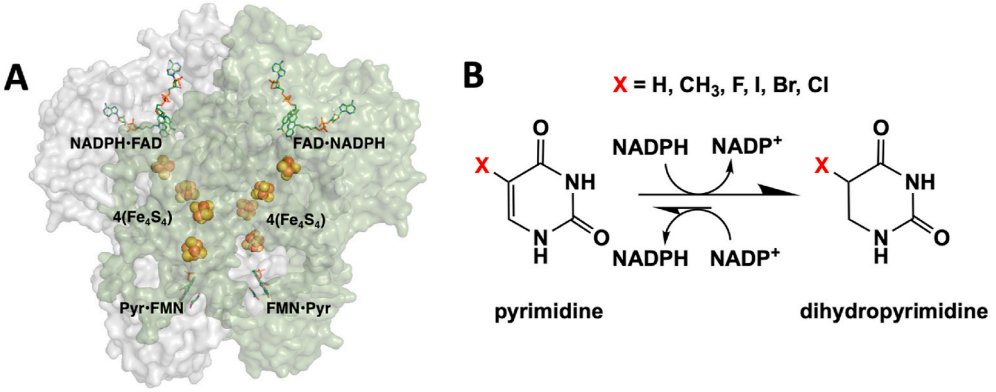

Fig. 1. Dihydropyrimidne dehydrogenase. **A**. The structure of DPD indicating the two subunits that comprise the dimer and the cofactor/substrate binding sites. **B**. The chemistry catalyzed by DPD.

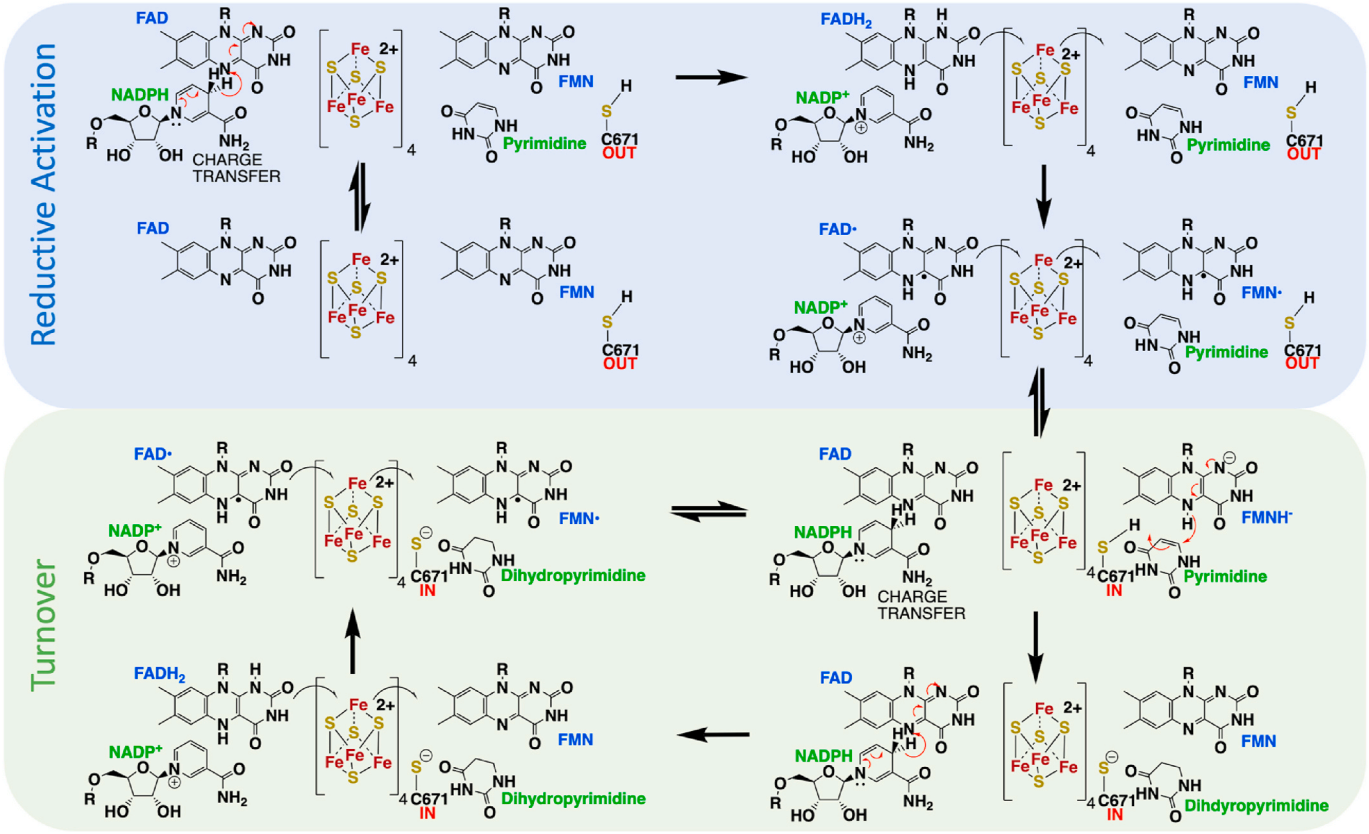

Scheme 1. The proposed mechanisms of reductive activation and turnover of mammalian dihydropyrimidne dehydrogenase. Reversible steps include ligand exchange.

centrifugal concentration using a 10 kDa cut-off filter (Amicon) and subsequent dilution to the target concentration. All preparative steps were performed at 4 °C.

2.3. Anaerobic methods

Kinetic experiments in this study were carried out under anaerobic conditions. Alternating cycles of vacuum and pure argon were applied to enzyme samples contained inside glass tonometers to exchange the dissolved dioxygen gas. This protocol used a modified version of a common Schlenk line and published procedures [20]. Residual dioxygen was reduced to trace hydrogen peroxide by the inclusion of 1 mM dextrose with the enzyme in conjunction with 1 U/mL glucose oxidase that was added from a tonometer side arm once the exchange cycles were complete. Solutions that included substrates and products were made anaerobic in buffer containing 1 mM dextrose by sparging for 5 min with argon prior to the addition of 1 U/mL glucose oxidase. All reactions listed below were measured under anaerobic conditions at 20 °C using a stopped-flow spectrophotometer set to single mixing mode. All concentrations indicated for transient-state experiments are post-mixing. Unless otherwise stated all reactions were undertaken in 30 mM KPi pH 7.4 buffer.

2.4. Data acquisition and analysis

Single wavelength absorption data from net single turnover reactions in which NADPH is limiting were fit to linear combinations of exponentials according to Equation (1) using Kaleidagraph software (Synergy). In this equation A_{Ynm} is the absorbance at wavelength Y, ΔA_n is the change in absorption at wavelength Y, k_{obs} is the observed rate constant, t is time, and C is the absorbance at the completion of the reaction.

$$A_{Ynm} = \left(\sum_{n=1}^{x} \Delta A_n \left(e^{-k_{obsn} t} \right) \right) + C \quad (1)$$

Single wavelength absorption traces and datasets from time-dependent spectral acquisitions were also fit to descriptive models using the numerical integration routines available in KinTek Explorer software (KinTek Corp.). Spectral datasets acquired using charged coupled device (CCD) detection were first deconvoluted using singular value decomposition and contributions from noise were culled from the data also using KinTek Explorer software.

2.5. Capture of the NADPH•FAD charge transfer spectrum

When monitoring the accumulation and decay of the charge transfer species at 590 nm with the C671S variant enzyme in the presence of NADPH and uracil, a rapid accumulation of absorption followed by a biphasic decay is observed. To separate the absorption contribution of each charge transfer species, 30 μM DPD C671S was mixed with 28 μM NADPH and 200 μM uracil in 5 mM KPi pH 7.4. The reaction was monitored from 300 to 700 nm using a CCD detector. To achieve sufficient time resolution two datasets were collected, one for 0.0012–1.6 s and one spanning 0.0012–200 s. These data were then spliced together at 1.6 s and corrected for minor offsets at the junction. The combined data set was then fit to a linear three-step irreversible model using singular value decomposition. The resultant spectra were then subtracted to yield the absorption changes that occur in each phase observed. The absorbance changes at 590 nm were isolated as a slice from this dataset and plotted. This trace was fit to a linear combination of exponentials according to Equation (1).

2.6. NADPH titration to DPD C671S variant

To isolate the influence that NADPH has on the activation of DPD, the C671S variant was used. This form of DPD has exceptionally slow pyrimidine reduction with thymine as a substrate and so provides separation for reductive activation from the ensuing turnover phase. C671S (17.5 μM), was mixed with 100 μM thymine and 5–75 μM NADPH. The reactions were monitored at 340 nm to observe the consumption of NADPH and at 590 nm to observe the accumulation of NADPH•FAD charge transfer. All traces were fit to a linear combination of exponentials according to Equation (1).

2.7. $NADP^+$ titration to the DPD C671S variant

To ascertain the extent to which NADPH and $NADP^+$ compete for access to the FAD active site and to demonstrate the origin of charge transfer absorption, reductive activation was observed for a fixed NADPH concentration in the presence of a range of $NADP^+$ concentrations and saturating thymine. As stated, this form of DPD has exceedingly slow turnover with the thymine substrate [9] meaning that the reductive activation events can be observed separated in time from the ensuing pyrimidine reduction. The C671S variant (12 μM), was mixed with 100 μM thymine, 13 μM NADPH, and 0–100 μM $NADP^+$. The reactions were monitored at 340 nm and 590 nm and the data obtained at both wavelengths were fit to a linear combination of exponentials according to Equation (1).

2.8. Kinetic assessment of reductive activation effectors

To probe the influence of pyrimidine substrates and products on DPD reductive activation, 14 μM of the DPD C671S variant was mixed with 13 μM NADPH alone, and with 13 μM NADPH in the presence of pyrimidines (uracil or thymine, 100 μM) or dihydropyrimidines (DHU or DHT, 300 μM). The reactions were monitored at 340 and 590 nm using photomultiplier detection. Individual traces were fit to a linear combination of exponentials according to Equation (1).

2.9. Evidence for reversibility of the DPD reaction

Although the reversibility of the DPD reaction has been established [9], the effects of ingress of electrons from dihydropyrimidines on the oxidation state of DPD has not been observed. Evidence for reduction of DPD by dihydropyrimidines was obtained by mixing 15 μM DPD C671S variant with 300 μM DHU with or without 300 μM $NADP^+$. A relative high concentration of $NADP^+$ was used to, trap by competition exchange NADPH formed from electrons supplied by DHU. Flavin reduction was monitored at 450 nm using photomultiplier detection. When DPD was mixed with only DHU the reaction was monitored from 0.0012 to 10 and from 0.0012 to 5000 s and these two datasets were spliced together at 10 s. At the conclusion of each measurement, a spectrum of the reaction mixture was collected from 300 to 600 nm. The difference spectrum for early events was obtained by subtracting the t_{zero} spectrum (that was collected prior to mixing) from the spectrum acquired at 10 s. The 10 s spectrum was then subtracted from the 5000 s spectrum to reveal the absorption changes that occur at longer times. A similar analysis was performed when DPD was mixed with DHU and $NADP^+$. The reaction was monitored for 10 and 3600 s and spliced as above to obtain a single dataset with sufficient temporal resolution for all events observed.

2.10. Crystallization of DPD (dihydro)thymine complexes

Crystals of DPD variant C671S were obtained using published protocols [18] that were adapted from Dobritzsch et al., 2001 [11]. DPD variant C671S (39.2 μM) in 25 mM HEPES, 2 mM DTT, 10% glycerol at pH 7.5 was mixed 1:1 with well solution containing 100 mM sodium citrate, 2 mM DTT, 19% PEG 6000 at pH 4.7 to yield a 6 μL drop. Crystallization was carried out in the dark to prevent photo-degradation of the somewhat dissociable FMN cofactor [21]. Under these conditions DPD crystals appeared within 16 h and were left to grow for additional 24 h. Crystals grew as single elongated rectangular hexahedrons (200 × 50 × 50 μM). Ligands were combined with the crystals under near anaerobic conditions as follows: before being placed in a Plas-Labs 830 series glove box, the well solution beneath selected crystallization drops was made anaerobic with the addition of dithionite to 10 mM and resealed with the cover slide. Crystals trays were placed in the glove box that contained a Motic binocular microscope coupled to an Accuscope 1080p high-definition camera. The glove box was sealed and made quasi-anaerobic by flushing with high-purity nitrogen gas for approximately 10 min at which time fractional dioxygen was recorded as 0.1%, by a Forensics Detectors oxygen meter. Atmospheric dioxygen was measured throughout the soaking procedure and was held <1%. C671S DPD crystals were soaked for a minimum of 20 min with DHT (R,S) (200 μM), DHT (R,S) (200 μM) with NADPH (100 μM), or with thymine (100 μM), each dissolved in the following cryo-solution: 20 mM sodium citrate, 0.4 mM DTT, 20% PEG 6000, 20% PEG 400, pH 7.5. The crystals were then submerged in liquid nitrogen, removed from the anaerobic environment, and stored under liquid nitrogen.

Diffraction data were collected at 100 K at the beamline 21-ID-D of the Advanced Photon Source at Argonne National Laboratory. The beamline was equipped with a Dectris Eiger 9 M detector. Data were collected using an oscillation angle of 0.5° over a range of 240° and an exposure time of 0.125 s per frame. The wavelength was fixed at 1.127 Å. Diffraction images were processed using autoPROC. Data processing statistics are given in Table 1. Phasing was conducted via molecular replacement using the program phaser. A model of Porcine DPD (PDB ID 7LJT) was used as a starting search model. The model building and refinement was undertaken in Coot and Phenix respectively in a repeated manner until the lowest Rfree was achieved. The coordinates and structure factors have been deposited in the Protein Data Bank with accession codes 8F5W, 8F61, and 8F6N (Table 1). Structural analysis and figures are made using PyMOL Version 2.0 (Schrödinger, LLC.).

2.11. The influence of the pyrimidine 5-substituent on the rate of hydride transfer

To observe the effect of the substituent at the 5-position of the pyrimidine, 5-halogenated pyrimidines were used as substrates. DPD C671S (10 μM) was mixed with 8 μM NADPH and 100 μM uracil, 5FU, 5ClU, 5BrU or 5IU and were each monitored at 340 and 590 nm. The influence of the substituents on the rate of pyrimidine reduction was most clearly observed in the second phase at 590 nm. These values were then used to fix the rate constants for this phase at other wavelengths. The log of the relative rates obtained for pyrimidine reduction were plotted against sigma values for this series of pyrimidines determined by Goyal et al. [22].

3. Results and discussion

Mammalian dihydropyrimidine dehydrogenase is an enigmatic enzyme. No explanation has yet been offered accounting for its size and complexity. The use of a single flavin cofactor for dehydrogenase chemistry is common [23–26] and such an arrangement is observed for class 1a dihydroorotate dehydrogenases (DHOD 1a) that accomplish very similar chemistry to that of DPD, but in pyrimidine biosynthesis [14,25]. Interestingly, domain IV of DPD (322/1025 residues) has the same fold and cofactor as DHOD 1a enzymes, adding to the perception of apparent unnecessary complexity for DPD [2].

The reaction sequence of DPD is quite unexpected. In the presence of NADPH and pyrimidine the oxidized enzyme is observed to take up two electrons from NADPH and reduce the FMN cofactor via the FAD and iron-sulfur centers as an initial activation process before pyrimidine reduction. Once activated DPD will not reoxidize in the absence of

Table 1
Data collection and refinement statistics.

PDB Code	8F61 (DHT)	8F6N (Thymine)	8F5W (DHT/NADPH)
Data Processing			
Wavelength (Å)	1.127	1.127	1.127
Resolution range (Å)	60.56–2.143	26.89–2.121	42.85–1.1972
Space group	P1211	P1211	P1211
Unit cell dimensions (Å)	81.784 157.667 162.564	82.445 158.144 165.707	81.735 158.003 162.404
Unit cell angles (°)	90.0 95.932 90.0	90 96.777 90	90 96.0562 90
Total reflections	439077	713645	1123295
Unique reflections	118212	146143	283435
Multiplicity	3.7 (3.6)[a]	4.9 (5.4)	4.0 (4.0)
Completeness (%)	89.3 (55.9)	88.0 (44.7)	98.6 (95.2)
Mean I/Sigma(I)	7.2 (2.0)	7.3 (1.6)	10.0 (1.1)
Wilson B-factor	26.04	29.82	23.08
[b]R_{pim}	0.103 (0.459)	0.091 (0.548)	0.075 (0.559)
[c]$CC_{1/2}$	0.989 (0.485)	0.990 (0.433)	0.994 (0.610)
Refinement			
[d]R_{work}	0.1870 (0.2724)	0.1824 (0.2429)	0.1787 (0.2578)
[e]R_{free}	0.2298 (0.3436)	0.2442 (0.3184)	0.2170 (0.2998)
Number of Non-Hydrogen Atoms	32219	31607	32519
Macromolecules	30922	30514	30850
Ligands	500	500	692
Solvent	797	593	977
[f]RMS(bonds) (Å)	0.006	0.039	0.009
RMS(angles) (°)	1.36	2.72	1.74
Ramachandran favored (%)	94.40	90.73	96.04
Ramachandran allowed (%)	4.93	7.94	3.64
Ramachandran outliers (%)	0.67	1.34	0.32
Average B-factor (Å^2)	33.40	40.24	32.60
Macromolecules (Å^2)	33.64	40.51	32.69
Ligands (Å^2)	24.94	27.01	32.67
Solvent (Å^2)	29.30	37.15	29.72

[a] The values for the highest-resolution bin are in parentheses.
[b] Precision-indicating merging R.
[c] Pearson correlation coefficient of two "half" data sets.
[d] $R_{work} = \Sigma|F_{obs} - F_{calc}|/\Sigma F_{obs}$.
[e] Five percent of the reflection data were selected at random as a test set, and only these data were used to calculate R_{free}.
[f] Root-mean square deviation.

NADPH even in the presence of excess oxidant pyrimidine. Pyrimidine reduction at the $FMNH_2$ cofactor site can only occur in the presence of NADPH, presumably so that the activated state is certain to be reinstated with each turnover (Scheme 1). The reduction of the pyrimidine is dependent on the conformational state of a dynamic loop at the $FMNH_2$ site that both gates access and carries the general acid cysteine required to protonate C5 of the base during hydride transfer from the $FMNH_2$ to C6. These highly novel reaction sequences require inter-active site communication, but no conformational evidence exists that would indicate the means by which occupancy of ligand binding sites is conveyed ~60 Å between the two active sites [1,10,11,17,18]. Structural and kinetic evidence suggests that reductive activation biases the average position of the dynamic loop at the $FMNH_2$ site such that it is more often proximal to the base in an inward position (Scheme 1) [18].

From an observational standpoint, the DPD reaction sequences are challenging to study. In addition to the requirement for anaerobic conditions, single turnover reactions are least ambiguous when NADPH is limiting. The reason for this is that excess NADPH will reduce DPD at a rate slower than the rate of turnover, resulting in an inability to recognize the reaction endpoint. However, limiting NADPH concentration results in one half the NADPH being committed to reductive activation and the residual to pyrimidine reduction on the now activated subunits such that only half of the expected engagement of the enzyme is observed. This successive enlistment of the same subunits was previously rationalized as arising from exceedingly high affinity for NADPH in the activated state such that the remaining NADPH is sequestered and unavailable to effectively activate other non-activated subunits. This model accounts for the data observed from the perspective of a single subunit but is not supported by direct evidence and this phenomenon has remained one of the aspects of the DPD reaction that is unaccounted for by experiment [9,17].

The catalytic engagement of enzyme equivalent to one-half of the limiting NADPH concentration is compounded for transient-state observations by the highly chromophoric character of the enzyme. The optical density of DPD solutions is such that concentrations above ~30 μM exceed the linear response of the stopped-flow spectrophotometer when using a 10 mm pathlength. As such, a maximum of ~15 μM enzyme can be observed to do chemistry given that half the NADPH is committed to reductive activation. In addition, specific steps of the chemistry can only be inferred as reduced states for the FAD and iron-sulfur centers have not been observed in normal catalysis suggesting that they decay rapidly relative to the rates of reductive (re)activation and pyrimidine reduction.

Despite these observational limitations there are characteristics of DPD that aid transient-state observation. The chemistry that occurs yields an abundance of subtle changes in the enzyme spectrum that are individually recognizable from signature difference spectra [9]. Reduction of FMN, charge transfer absorption for the NADPH•FAD complex, characteristic perturbations of the flavin spectra that occur with changes in ligand state added to oxidation of NADPH, collectively provide quite explicit evidence of the underlying chemical sequence. Here and in prior studies we have exploited these spectrophotometric signals in addition to product analyses and evidence of enzyme and pyrimidine oxidation states in X-ray crystal structures to elaborate a reasonably complete description of the DPD reaction (Scheme 1).

3.1. Deconvolution of charge transfer absorption

Three events are observed when DPD saturated with pyrimidine is mixed with a limiting concentration, with respect to the enzyme, of NADPH. These events can be observed at all wavelengths between 300 and 700 nm but two wavelengths have proven routinely diagnostically useful. As a result of reduced states of FAD and the iron-sulfur centers not accumulating during activation or catalysis, 340 nm reports primarily oxidation of NADPH [9]. Long-wavelength charge transfer absorption can be observed relatively independently beyond the absorption of the flavin cofactors at around 590 nm (Fig. 2A).

At 590 nm three phases are observed in net single turnover reactions. The first is assigned as rapid association of NADPH to localize adjacent to the FAD isoalloxazine. A decrease of this charge transfer absorption occurs concomitant with reductive activation and has been tentatively ascribed to formation of a second NADPH•FAD complex by exchange once electrons used to activate the enzyme have shuttled to the FMN cofactor. The final phase observed is one catalytic cycle in which the pyrimidine substrate is reduced and the $FMNH_2$ state is reinstated by oxidation of all remaining NADPH at the FAD site followed by electron transfer to the FMN. As mentioned above, aspects of this process remain difficult to account for. In particular, that half the limiting NADPH included in single turnover reactions is consumed in reductive activation and the remainder in turnover [9]. This occurs despite that activation is more rapid than the ensuing pyrimidine reduction and therefore it would be expected that a majority of the limiting NADPH would be consumed in the reductive activation process.

To establish that both the first and second intermediates observed at 590 nm report charge transfer, reductive activation of the C671S variant enzyme at high enzyme concentration and in the presence of saturating uracil was observed. This form of the enzyme is catalytically competent and so is expected to consume all added NADPH in the presence of excess pyrimidine. It also kinetically delineates the reductive activation and pyrimidine reduction phases to a greater extent than WT DPD and so

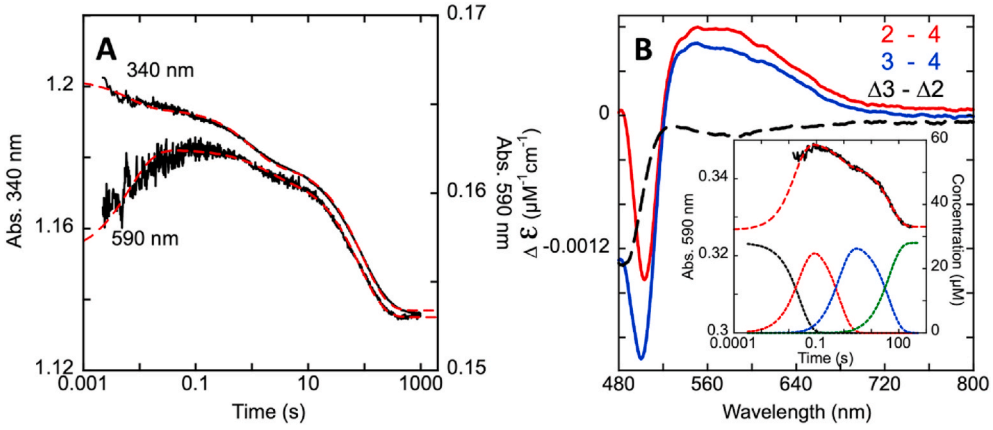

Fig. 2. Charge transfer absorption in single turnover reactions of DPD C671S. **A.** Representative absorption changes at 340 and 590 nm when C671S DPD (15 μM) was mixed under anaerobic conditions with NADPH (13 μM) and uracil (100 μM). These data were fit to a linear combination of three exponentials according to Equation (1). **B.** Spectral deconvolution of charge transfer absorption. DPD C671S (30 μM) was mixed with NADPH (28 μM) and uracil (200 μM). CCD data were collected for two timeframes (0.0012–1.6 s & 0.0012–200 s) and spliced together at the limit of the shorter acquisition. The resulting dataset was fit to a three-step linear irreversible model using the singular value decomposition routine available in KinTek Explorer. The spectra shown are the difference spectra for the second (red spectrum) and third (blue spectrum) species. **Inset** depicts a slice extracted at 590 nm showing formation and biphasic decay of the charge transfer absorption overlaid with the predicted species accumulation profile in dashed lines. The black dashed line is decay of the NADPH•DPD•U state, the red dashed line is formation and decay of the first charge transfer complex, blue dashed line is formation and decay of the second charge transfer complex, and green dashed line is formation of the $NADP^+$•DPD•DHU complex.

the first and second intermediate states show high fractional accumulation and are observed to form in well separated phases. Using CCD detection, the spectral dataset was deconvoluted using singular value decomposition to obtain the spectra for the two transient-states (Fig. 2B). The data were fit to a linear irreversible three-step model and were described well with rate constants of 60 s^{-1}, 1.45 ± 0.09 s^{-1} and 0.020 ± 0.001 s^{-1}. The initial rate constant, however, was not defined from these data and was fixed to an estimate of 60 s^{-1} in this and other experiments in this study. The latter two rate constants were defined from the fit and agree well with prior observations with this variant [9]. Given that charge transfer absorption decays completely with oxidation of all available NADPH, the difference spectra were obtained by subtracting the final spectrum from the spectra for the intermediates. These difference spectra clearly show that the first and second transients have similar charge transfer absorption transitions and that the second is somewhat less intense (Fig. 2B). This is consistent with a model where initial NADPH binding forms a charge transfer complex comprised of NADPH•FAD•4(Fe_4S_4)•FMN•Pyr and repopulation with NADPH after reductive activation forms the NADPH•FAD•4(Fe_4S_4)•$FMNH_2$•Pyr complex producing a second similar charge transfer band prior to pyrimidine reduction. The decreased absorption of this species is likely a result of the now lower concentration of NADPH and competition for the FAD site with $NADP^+$ formed in the prior reductive activation phase (see Fig. 4).

3.2. Evidence for asymmetry in the DPD homodimer

As mentioned, a persisting curiosity regarding the consumption of NADPH is that for concentrations equal to or below that of the enzyme, one half of the added reducing substrate is consumed in the relatively rapid activation step and the remaining half is then consumed to reinstate the $FMNH_2$ during the ensuing reduction of the pyrimidine [9]. To further investigate the interaction of NADPH with DPD, the exceedingly slow pyrimidine reduction rate of the C671S variant with thymine as a substrate was employed. Relative short acquisition times with this variant in the presence of thymine only capture reductive activation to form the NADPH•FAD•4(Fe_4S_4)•$FMNH_2$•thymine state of the enzyme. When the variant enzyme was mixed with thymine and varied concentrations of NADPH, the 590 nm data indicate that the time required for maximal accumulation of charge transfer and the observed amplitude varies with NADPH concentration (Fig. 3A). Descriptively, the maximal accumulation of charge transfer appears to occur later and to higher absorbances when the concentration of NADPH exceeds that of the enzyme. Analytically, the data for these concentrations were best described by three exponential phases while data for lower concentrations (9.5 & 4.6 μM NADPH) could be fit adequately with two exponential terms (Fig. 3A and B).

The biphasic increase in absorption for NADPH concentrations in excess of the enzyme fit to a fixed rate of 60 s^{-1} followed by a rate of ~10–20 s^{-1}. That the second increase is apparent only with NADPH concentrations above that of the enzyme (>28.3 μM) suggests the involvement of the second subunit albeit with apparently weaker and slower association with NADPH. This pattern of NADPH oxidation could arise from having high and low affinity NADPH binding sites in each dimer such that only one subunit is available for activation. Another feature of the 590 nm data is that the amplitude of the last phase observed, reductive activation, is relatively constant. The amplitudes observed at 340 nm show evidence for why this is the case, in that the amplitude of the reductive activation phase for NADPH concentrations above 28.3 μM indicate a limit of ~9 μM NADPH oxidation, designating that half of the enzyme (17.5 μM) reductively activates despite having an excess of NADPH available.

Together these observations demonstrate asymmetry in the DPD dimer where only one of the two subunits is conformationally competent at any point in time. With slow turnover, such as is the case for the C671S variant with thymine, the second NADPH binding site can be observed to populate but only at high concentrations. One possibility is that the second subunit does not reductively activate until turnover has occurred in the previously reductively activated subunit. To test the validity of these hypotheses, the data shown in Fig. 3 were fit globally using numerical integration to a model consistent with asymmetry in the DPD homodimer for the steps of reductive activation only (Fig. S1). While the fit does not conform precisely to the 590 nm traces, the set of nested simulation curves for this wavelength do broadly describe the data. These data cannot accurately reveal the actual balance of affinities for the two sites for NADPH binding. The fit is therefore illustrative of

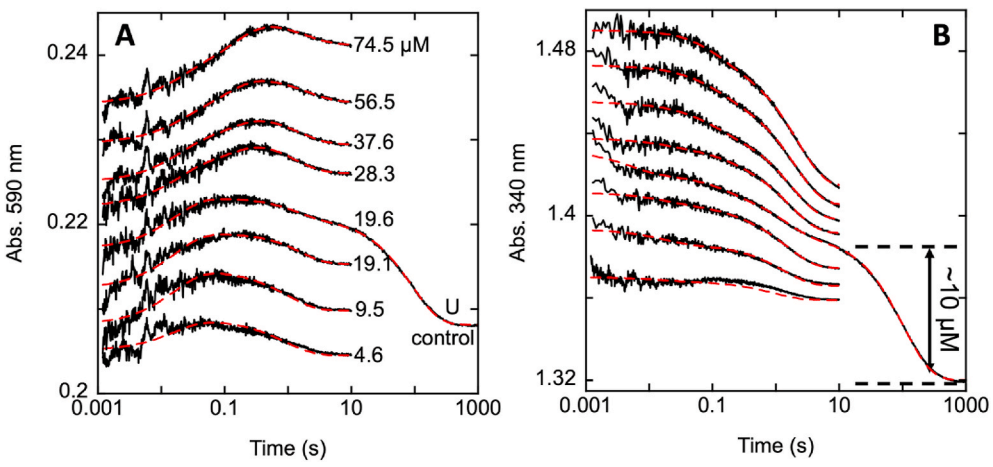

Fig. 3. NADPH titration to DPD C671S variant. For **A** & **B** DPD C671S (17.5 μM) was mixed under anaerobic conditions with thymine (100 μM) and varied NADPH (concentrations as shown in **A**). Both plots include a control using uracil as the oxidant substrate to verify competence in pyrimidine reduction. The data for 4.6 and 9.5 μM were fit to a linear combination of two exponentials according to Equation (1). Data for 19.1–74.5 μM were fit to a linear combination of three exponentials according to Equation (1). The control reaction with uracil was fit to four exponentials according to Equation (1). For each trace the initial rate was fixed to 60 s^{-1}, as this event is generally poorly captured in these data. **A.** Data recorded at 590 nm report FAD•NADPH charge transfer. **B.** Data at 340 nm primarily report NADPH oxidation. NADPH concentration increases from bottom to top. The traces in both plots were separated for clarity. In each the bottom trace is approximately representative of the actual absorbance.

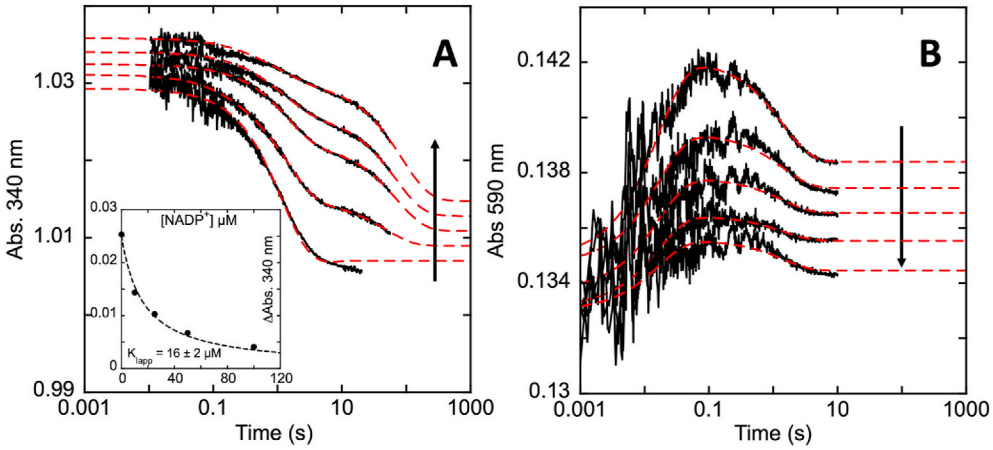

Fig. 4. Assessment of the relative binding affinity of NADPH and $NADP^+$ during reductive activation of the DPD C671S variant. DPD C671S (13 μM in **A.** and 12 μM in **B.**) was mixed under anaerobic conditions with thymine (100 μM), NADPH (13 μM) and varied $NADP^+$ (0, 10, 25, 50, 100 μM). **A.** The 340 nm data were fit for the analytical purpose of measuring the amplitude for the second phase. In each case the data were fit to three exponential terms and the rate for the first and second phases were fixed to 60 s^{-1} and 0.7 s^{-1} respectively. **Inset** shows the NADP $^+$ dependence of the decrease of initial amplitude for reductive activation divided by the extinction coefficient for NADPH oxidation fit to an inverted hyperbolic function to provide an apparent K_I as illustration of the competition for access to the NADPH binding site. For **B.** the 590 nm data were fit two exponential terms and the rate for the first and second phases were fixed to 60 s^{-1} and 0.7 s^{-1} respectively. For both **A** and **B** traces were separated for clarity. Arrows indicate increasing NADP $^+$ concentration.

data expected if there were bias toward population of one NADPH binding site over the other. This model for engagement of the second subunit accounts for half of the added NADPH being consumed in reductive activation and the other half in turnover for reactions in which NADPH is limiting. We therefore propose that the oxidized DPD dimer is asymmetric and utilizes an alternating subunit mechanism in which pyrimidine reduction on the conformationally active subunit is required to instigate reductive activation and turnover on what was the conformationally inactive subunit. This conclusion is drawn in part because the measured turnover number closely matches the rate constant of pyrimidine reduction and so incorporates the contribution of both subunits. However, in this model all sites are available for binding substrates and so both subunits register charge transfer but at differing rates.

Additional evidence supports an alternating subunit mechanism. In prior work, the position of the dynamic loop that carries the active site general acid cysteine and gates access to the pyrimidine binding site was observed to adopt both the inward and outward conformations in each dimer [18]. In addition, early DPD structures with 5IU clearly indicate two subunit states in each dimer [1]. Evidence for asymmetry is observed in the structures of DHT complexes discussed below. Furthermore, in earlier studies we showed flavin reduction in reductive activation equivalent to one half of expectation when using NADPH concentrations comparable to that of the enzyme [9]. And lastly, when DPD C671S crystals were incubated with excess NADPH in the presence of saturating thymine, both FMN cofactors were observed to be reduced, serving as evidence of the activation of both subunits [17]. While the reasons for sequential subunit activation are not apparent, it is conceivable that such a mechanism conserves NADPH utilization, suppressing engagement of both subunits when this substrate is limiting specifically to limit futile oxidation of the $FMNH_2$ cofactor by reaction with dioxygen.

3.3. *Binding competition between $NADP^+$ and NADPH*

The decreased extinction coefficient of the second charge transfer absorption with reductive activation shown in Fig. 2B is consistent with the $NADP^+$ formed during reductive activation now competing with NADPH for binding adjacent to the oxidized FAD that was reinstated with reduction of the FMN. To evaluate this competition, NADPH

oxidation and charge transfer accumulation was observed at a range of $NADP^+$ concentrations with the DPD C671S variant in single turnover with thymine (Fig. 4). Thymine reacting with this variant induces an estimated pyrimidine reduction rate constant of 0.00024 s^{-1} and so ostensibly isolates observation of the initial reductive activation event, that occurs at ~0.7 s^{-1} [9]. These data show that $NADP^+$ competes for binding with NADPH. This is evident both in the incrementally diminished accumulation of charge transfer absorption observed at 590 nm and at 340 nm in the separation of the reductive activation process into two phases (phases 2 & 3). The initial reductive activation phase can be fit using the same rate constant for each $NADP^+$ concentration (0.7 s^{-1}) but with incrementally smaller amplitude. This is direct evidence of fractional binding of NADPH as a result of competition for access to the FAD site. The subsequent phase presumably results from additional NADPH being drawn into the reductive activation process, albeit at a slower rate due to competitive binding with $NADP^+$. Qualitatively these data show that the amplitude associated with reductive activation is diminished by ~50% at roughly equal concentrations of NADPH and $NADP^+$ and therefore these ligands must have comparable binding affinities to the NADPX•FAD•4(Fe_4S_4)•FMN•Pyr state of the enzyme. The binding of $NADP^+$ can be observed in static titration as perturbation of the flavin spectrum and the measured dissociation constant is 4.3 ± 1.4 μM (data not shown). This experiment suggests NADPH has a similar, low micromolar affinity. Prior transient-state experiments using a variety of concentrations of enzyme and NADPH concentrations in the presence of saturating pyrimidine return reproducible measurements for rate constants when fit, which is qualitative evidence that low concentrations of NADPH give a good approximation of first order conditions as a result of high binding affinity. Nonetheless, the dissociation constants that define the competition for access to the FAD site cannot be determined reliably from these data. Moreover, it cannot be stated from these data that reductive activation modulates NADPH or $NADP^+$ binding, as we have proposed previously [9]. The conclusions available from this data added to prior kinetic modelling would suggest that NADPH binding is high affinity for both non-activated and activated states of the enzyme [9]. That the absorption of both charge transfer complexes can be diminished in intensity with added $NADP^+$, indicates that both $NADP^+$ and NADPH are free to exchange with the non-activated and activated forms of DPD. These observations minimally provide a clear explanation for $NADP^+$ formed during reductive activation contributing to the decrease in signal for the second charge transfer species observed (Fig. 2B).

3.4. Reductive activation effectors

We have proposed a mechanism for DPD in which the reductively activated form of the enzyme can only reduce pyrimidine substrates in the presence of both pyrimidine and NADPH. In this mechanism the first step in catalysis is reduction of the pyrimidine substrate with concomitant reductive reactivation to reinstate the active form of the enzyme ($NADP^+$•FAD•(Fe_4S_4)$_4$•$FMNH_2$•$PyrH_2$). One interesting extension of this mechanism is that reductive reactivation could also be stimulated by dihydropyrimidine as the effector molecule and so could occur as an integral part of one catalytic cycle (i.e. prior to dihydropyrimidine release). To test whether dihydropyrimidines can induce rapid (re) activation by NADPH, DPD C671S was mixed with limiting NADPH and saturating concentrations of pyrimidines or dihydropyrimidines. These data show that both DHU and DHT induce reductive activation at comparable rates to those observed for uracil and thymine, establishing that the dihydropyrimidine products are effectors and that in normal turnover reductive reactivation is stimulated by either the dihydropyrimidine product or pyrimidine substrate bound at the FMN site (Fig. 5). NADPH alone can reduce DPD, but at rates too slow to support the turnover number with uracil for this variant. Such a mechanism would ensure that the enzyme returns to its active form with each turnover irrespective of the availability of pyrimidine substrates. In Fig. 5B we show the accumulation and decay of NADPH•FAD charge transfer absorption during reductive activation (and pyrimidine reduction where applicable). The data acquired at 590 nm show, as might be expected, that NADPH binds with a similar rate regardless of ligand occupancy of the FMN-pyrimidine site. For DHU and DHT reductive reactivation is stimulated and no further reaction is possible and so we observe sustained, albeit weaker, charge transfer for these ligands as the FAD site is repopulated by the residual NADPH. As stated, for thymine with this variant, pyrimidine reduction is exceedingly slow and so the trace obtained appears similar to those for DHU and DHT for times ≤10 s. Only the trace obtained at this wavelength for uracil exhibits three phases. The first phase being NADPH binding, the second reductive activation and the third is one catalytic cycle where reduction of the uracil concomitant with reductive reactivation consumes all residual NADPH resulting in the complete loss of charge transfer transitions.

3.5. Evidence for dihydropyrimidines as reducing substrates

We have demonstrated that the chemistry catalyzed by DPD is biased toward NADPH oxidation and pyrimidine reduction by ~10 kJ/mol [9]. In other words, in reactions that include equal concentrations of NADPH and pyrimidine or $NADP^+$ and dihydropyrimidine the formation of dihydropyrimidine is biased ~20-fold over pyrimidine. Dihydropyrimidine as a reducing substrate requires that the electrons liberated traverse the DPD cofactor set in the opposite direction. That the FAD and iron-sulfur centers are only ever observed as oxidized during pyrimidine

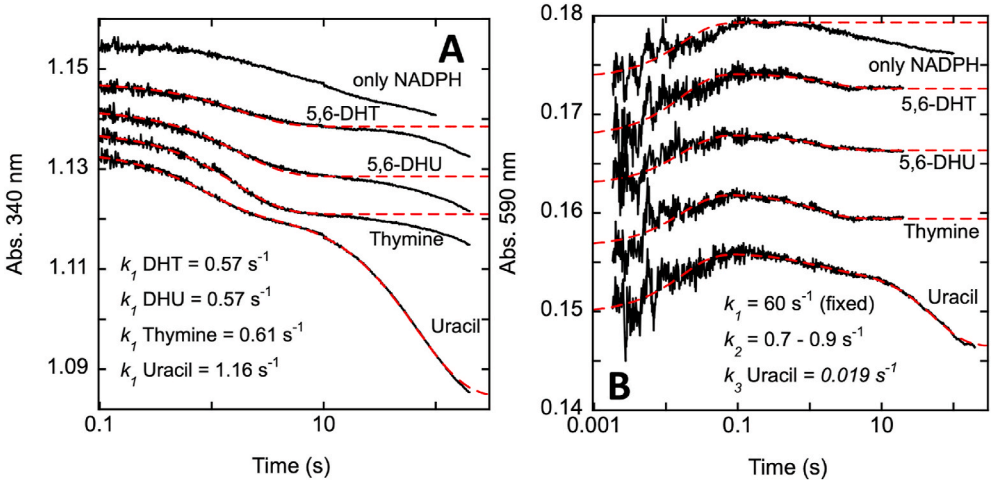

Fig. 5. Kinetic assesment of reductive activation effectors. DPD C671S variant (14 μM DPD) was mixed under anaerobic conditions with NADPH (13 μM) and pyrimidines (uracil or thymine, 100 μM) or dihydropyrimidines (dihydrouracil (DHU) or dihydrothymine (DHT), 300 μM) and observed at 340 nm that reports NADPH oxidation (**A**) and 590 nm that shows the development of charge transfer absorption arising exclusively from proximity of the NADPH and FAD (**B**). Specific phases or sets of phases were fit to linear combinations of exponentials according to Equation (1). The traces in each plot were separated for clarity.

reduction catalysis implies that these cofactors have lower reduction potentials than that of FMN and that the iron-sulfur center conduit provides a flat energy surface for electron transmittance. In such a descriptive model, reduced states of either the FAD or the iron-sulfur centers do not accumulate in catalysis in either direction with the enzyme's architecture facilitating electron migration to the FMN cofactor. Electrons on the $FMNH_2$ will have some limited propensity to move between the two flavins but more often reside on the $FMNH_2$ and only transiently on the iron-sulfur centers and FAD.

To study the process of the dihdropyrimidine oxidation chemistry we mixed oxidized, non-activated DPD with dihydrouracil, with and without saturating $NADP^+$. The $NADP^+$ serves both as an oxidant substrate and a means to compete off, and therefore retain, NADPH formed. In Fig. 6A a saturating concentration of DHU and DHU with $NADP^+$ were mixed with the C671S variant enzyme and the reaction was monitored at 450 nm. In the presence of DHU alone, a small amount of flavin is observed to reduce at a rate that is substantially slower than that of reductive activation of this variant with NADPH and pyrimidine. In the presence of $NADP^+$ and DHU an increase in NADPH absorption is observed without distinct evidence of flavin reduction. Even when observing the reaction for 14 000 s in the presence of $NADP^+$, no evidence of reduced flavin can be discerned from flavin perturbations arising from ligand binding (ca Fig. 6B and C) [9]. This demonstrates that the completion of the electron conduit with the introduction of $NADP^+$ will draw electrons into the enzyme from dihydropyrimidine in much the same but converse manner for the forward reaction.

One additional curiosity of DPD is that the difference spectra observed for $NADP^+$ and pyrimidine binding are similar and therefore changes in absorbance when both are present appear additively larger (Fig. 6B). Similar to the forward reaction, no evidence of reduced Fe_4S_4 centers is observed in the absorption spectra. Additionally, at 450 nm, the DHU only trace appears to have limited progression at 3000 s and the trace with $NADP^+$ present does not come to completion within 6500 s. Furthermore, no charge transfer is evident in any of the difference spectra collected, consistent with any NADPH generated being competed off the enzyme in the presence of $NADP^+$. Following these reactions to endpoints is not feasible in that even after 14 000 s only a fraction of available $NADP^+$ had been reduced. However, it is reasonable to conclude that given sufficient time that the enzyme in the presence of DHU alone would undergo reductive activation. In the presence of both $NADP^+$ and dihydrouracil only the small fraction of electrons on the dihyropyrimidine with sufficient energy to reduce the distant $NADP^+$ traverse the enzyme, none apparently accumulating on a reduced state of a flavin.

3.6. Structural evidence for DHT as a substrate

Dobritzsch et al. were the first to obtain a crystal structure of dihydropyrimidine dehydrogenase [1,11] and their data and analyses were the first definitive evaluation of the cofactor arrangement. Several substrate/inhibitor complexes have since been solved including, the NADPHDPD•5FU complex [11], the DPD•5IU complex, the NADPH•DPD•5IU complex, the NADPH•DPD•uracil-4-acetic acid complex [1], the DPD•5-ethynyluracil (5EU) complex, and the NADPH•DPD•5EU complex [18]. The structures solved with 5EU have confirmed the proposed steps of reductive activation quite clearly and these steps were also apparent in the NADPH•DPDC671S•thymine complex structure that revealed the activated form of the enzyme is reduced at the FMN cofactor [17]. In an attempt to solve the structures of DPD bound to dihydropyrimidine we briefly soaked DPD C671S crystals with thymine, (R,S)DHT, and (R,S)DHT with NADPH under anaerobic conditions see Table 1.

The structures obtained show, as is indicated in Fig. 6, that dihydropyrimidines can reduce DPD in that both structures solved with added DHT have half of the active sites of the four subunits in the asymmetric unit housing thymine. As a control, the crystal structure of the DPD•thymine complex was also solved and has clear in-plane density for the 5-methyl of the thymine (Fig. S2). For the structure derived from soaking with DHT it was observed that for one subunit of each dimer the electron density reflects a thymine molecule and the other subunit contains a DHT, again indicative of alternating subunit reactivity (Fig. 7). Corresponding structural evidence of FMN reduction in the thymine bound active sites could not be discerned at the resolution achieved. The shape of electron density for thymine is shown in subunits A and D in Fig. 7 and in Fig. S3. Conversely subunits B and C are lacking electron density at the C5 position (Fig. 7). The basis for concluding that the absence of density for the 5-methyl substituent of the DHT is evidence of unreacted DHT is that the out-of-plane methyl group has no interaction partner within the protein. This lack of constraint likely resolves to indicate little density and may also be diminished by averaging with the S-isomer that is present in the racemic mixture of added DHT. Moreover, the NADPH•DPD•5IU structure solved by Dobritzsch et al., also indicated only uracil bound in the active site of one subunit in each dimer. Presumably reduction of 5IU to 5-iodoDHU brought about a similar crystallographic artifact given that displacement of the iodo-group would only occur with crosslinking to the active site general acid cysteine and this was observed in the other subunit of each dimer [1].

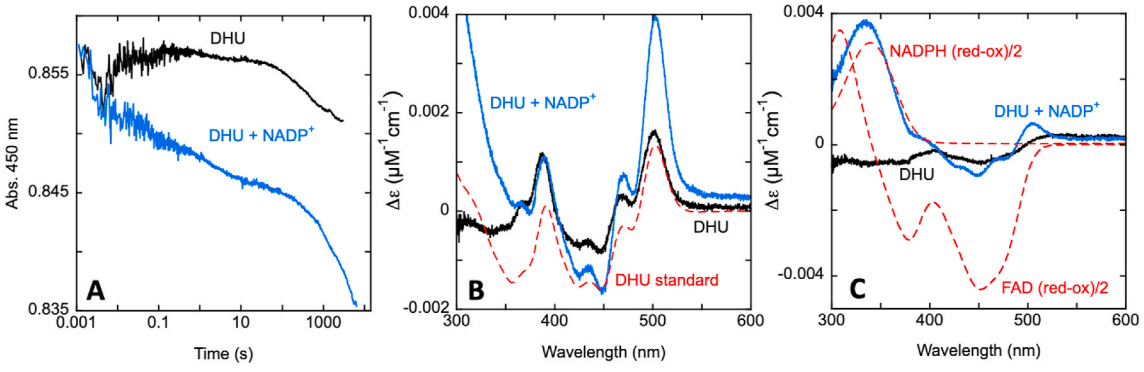

Fig. 6. Spectrophotometric evidence for dihydropyrimidine as a reductant substrate. C671S DPD (12 μM) was mixed under anaerobic conditions with DHU (300 μM) and with or without $NADP^+$ (300 μM). **A.** The absorption changes observed at 450 nm. **B.** The difference spectra for t = 10 s minus the spectrum for unliganded DPD. The spectrum shown in red dashes is a reference difference spectrum for DHU binding. **C.** The difference spectra for t = 3000 minus t = 10 s for DHU only and t = 14000 minus t = 10 s for DHU and $NADP^+$. The spectra shown in red dashes are for reference and indicate one half the expected changes for flavin reduction and $NADP^+$ reduction.

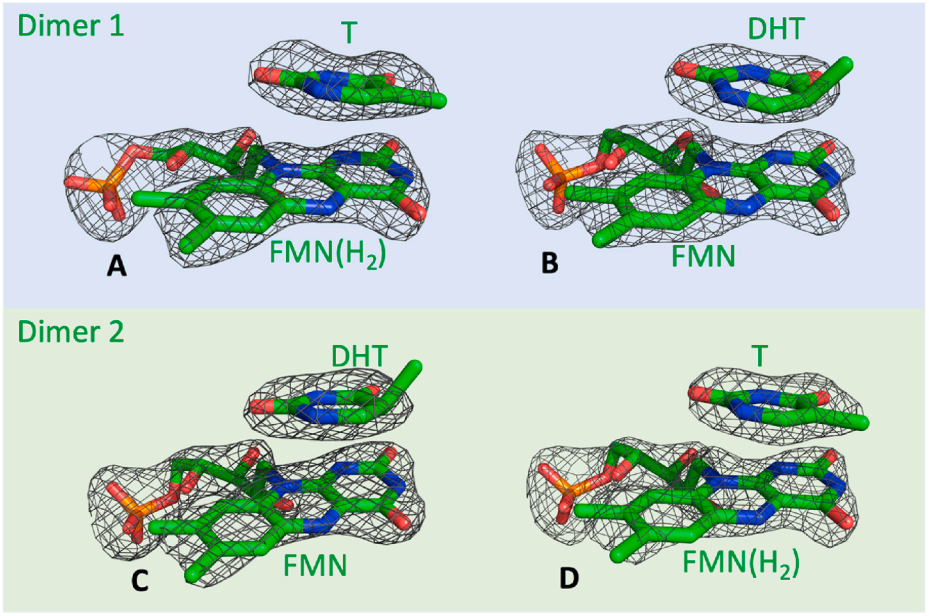

Fig. 7. FMN active site of DPDC671S•DHT complex. Subunits A and B compose dimer 1 (blue rectangle). Subunits C and D compose dimer 2 (green rectangle). The polder map density of the FMN and thymine/DHT of each subunit is displayed individually at 5.0 s.

3.7. The influence of the pyrimidine 5-substituent on the rate of hydride transfer

Hydride transfer from $FMNH_2$ to pyrimidine substrate is rate limiting for uracil and thymine [9]. However, thymine reduction is twofold slower than uracil with the WT enzyme and ~50-fold slower than uracil with the C671S variant [9]. The origin of these relative hydride transfer rates is unclear and suggests that substrate reactivity in the complex is one of a number of factors defining the rate of hydride transfer. To investigate effects of the substituent at the 5-position of uracil a series of 5-halogenated uracils were studied as substrates for the C671S form of DPD. This variant has been shown to slow pyrimidine reduction (coupled to reductive reactivation) to a greater degree than the initial reductive activation, thus delineating these events and so observationally isolating hydride transfer to the pyrimidine from other processes. Fig. 8 depicts the reaction of DPD with limiting concentrations of NADPH and near saturating 5-substituted uracils. The data obtained are typical of DPD single turnover reactions albeit with slightly altered appearance for the 5-halo-pyrimidines for which the rate of pyrimidine reduction rivals that of reductive activation so that these events blend to various extents at 340 nm. The 590 nm signals decay with oxidation of NADPH that occurs with both reductive activation and reductive reactivation coupled to turnover. This later process provides an objective measure of the rate of pyrimidine reduction that does not compete with other signals [17].

The first phase observed at 590 nm reports the binding of NADPH to the FAD active site and thus shows no evidence of modulation by the pyrimidine 5-substitutuent bound at the distant FMN site. As might be expected the rates for decay of the 590 nm signal, that corresponds to complete consumption of NADPH with pyrimidine reduction, show that decreasing the electron density at the 6-carbon of the pyrimidine of electrons promotes the pyrimidine reduction hydride transfer reaction and that the dependence of $\log(k/k_0)$ is linear with the reported sigma (−) value for the series [22]. Also expected is that the slope has a positive rho value indicative of negative charge accumulation in the transition state. This is both consistent with an early transition state for nucleophilic hydride transfer and importantly the linearity suggests that steric factors at the 5-position do not influence the observed rate to any appreciable extent up to the radius of an iodo group that has a volume comparable to that of the thymine 5-methyl. This trend is also consistent with the modest electron donation provided by the thymine 5-methyl and the corresponding slower rate of pyrimidine reduction observed. However, the data does not explain why the hydride transfer to thymine is decreased by 50-fold compared to uracil in the C671S variant and only

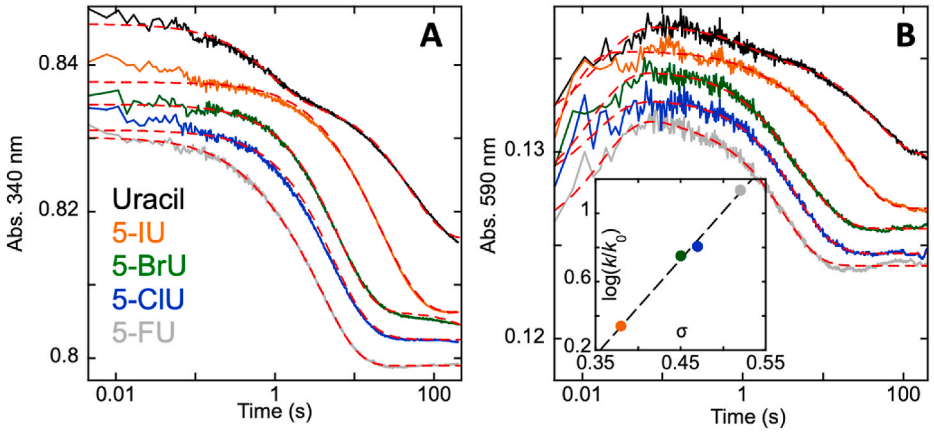

Fig. 8. DPD single turnover with 5-substituent pyrimidines. C671S DPD (10 μM) was mixed under anaerobic conditions with NADPH (8 μM) and 5XU (100 μM) and observed at 340 (**A**) and 590 (**B**) nm where X is H (black traces), I (brown traces), Br (green traces), Cl (blue traces), and F (grey traces). The inset in C is a Hammet analysis based on s values obtained from reference [22]. The data at 340 nm were fit to a linear combination of two exponentials while the 590 nm data were fit to three. The traces in both plots were separated for clarity.

twofold in the WT. Overall it can be concluded that the methyl substituent of thymine impedes the rate of hydride transfer by weak electron donation but that its volume does not play a role.

This data also offers very clear evidence for why DPD is such an effective catalyst for 5-fluorouracil (5FU) reduction. 5FU is one of the most-commonly prescribed chemotherapeutics and is effective against a broad array of cancers [27,28]. The activity of DPD undermines 5FU treatment by essentially eliminating efficacious toxicity within 30 min of administration [29]. The data show that 5FU increases the rate of turnover in the C671S variant by ~ tenfold. The WT enzyme however, exhibits a nearly identical rate of turnover with 5FU (0.61 s^{-1}) as that for U (0.59 s^{-1}) (data not shown) accounting for the rapid rate of detoxification observed in cancer patients and the need for ambulatory pumps to supply continuous 5FU dosages over multiple days to achieve efficacious net toxicity.

3.8. Conclusions

In recent publications we have revealed quite unexpected and novel catalytic sequences in the reaction catalyzed by DPD. While we have defined accurate descriptions for most, aspects of the enzyme's behavior had remained unclear. In this study we have sought to address some of the enigmatic aspects of the catalytic function of DPD using observation of weak charge transfer signals that arise and then decay during reductive activation and turnover. These signals are assigned to occur with the proximity of the NADPH dihydronicotinamide and the FAD isoalloxazine. In single turnover we have consistently observed for DPD that regardless of the NADPH concentration, only one half is consumed in reductive activation and one half is consumed during turnover. This curious behavior is partly accounted for with the model presented here. We tentatively propose that the DPD dimer is asymmetric. Only one subunit of DPD is available to activate and then turnover and the other subunit can bind substrates but does not adopt an active conformation until the subunit first engaged completes turnover. The evidence for this is shown in Fig. 3 and S1 and while not definitive, the data was largely recapitulated with a model that has two distinct states for subunits within the dimer (Fig. S1). We also show that dihydropyrimidines are positive effectors for reductive activation. The mechanistic conclusion drawn from this observation is that backfilling of electrons to reinstate the active form of the enzyme can occur as part of the current catalytic cycle and is possibly the reason why pyrimidine reduction is contingent on occupancy of the NADPH binding site; to ensure reinstatement of the active enzyme with each turnover. We also show that the volume difference between uracil and thymine at the 5-position of the pyrimidine does not influence the rate of pyrimidine reduction and that other factors must be at play to modulate the rate of the pyrimidine reduction step.

Data availability

Data will be made available on request.

Acknowledgements

This research was supported by National Science Foundation Grants 1904480 and 2203593 to G.R.M.

Appendix A. Supplementary data

Supplementary data to this article can be found online at https://doi.org/10.1016/j.abb.2023.109517.

References

[1] D. Dobritzsch, S. Ricagno, G. Schneider, K.D. Schnackerz, Y. Lindqvist, Crystal structure of the productive ternary complex of dihydropyrimidine dehydrogenase with NADPH and 5-iodouracil. Implications for mechanism of inhibition and electron transfer, J. Biol. Chem. 277 (2002) 13155–13166.
[2] K.D. Schnackerz, D. Dobritzsch, Y. Lindqvist, P.F. Cook, Dihydropyrimidine dehydrogenase: a flavoprotein with four iron-sulfur clusters, Biochim. Biophys. Acta 1701 (2004) 61–74.
[3] K. Rosenbaum, K. Jahnke, B. Curti, W.R. Hagen, K.D. Schnackerz, M.A. Vanoni, Porcine recombinant dihydropyrimidine dehydrogenase: comparison of the spectroscopic and catalytic properties of the wild-type and C671A mutant enzymes, Biochemistry 37 (1998) 17598–17609.
[4] B. Lohkamp, N. Voevodskaya, Y. Lindqvist, D. Dobritzsch, Insights into the mechanism of dihydropyrimidine dehydrogenase from site-directed mutagenesis targeting the active site loop and redox cofactor coordination, Biochim. Biophys. Acta 1804 (2010) 2198–2206.
[5] B. Podschun, P.F. Cook, K.D. Schnackerz, Kinetic mechanism of dihydropyrimidine dehydrogenase from pig liver, J. Biol. Chem. 265 (1990) 12966–12972.
[6] B. Podschun, K. Jahnke, K.D. Schnackerz, P.F. Cook, Acid base catalytic mechanism of the dihydropyrimidine dehydrogenase from pH studies, J. Biol. Chem. 268 (1993) 3407–3413.
[7] D.J. Porter, T. Spector, Dihydropyrimidine dehydrogenase. Kinetic mechanism for reduction of uracil by NADPH, J. Biol. Chem. 268 (1993) 19321–19327.
[8] K. Rosenbaum, B. Schaffrath, W.R. Hagen, K. Jahnke, F.J. Gonzalez, P.F. Cook, K. D. Schnackerz, Purification, characterization, and kinetics of porcine recombinant dihydropyrimidine dehydrogenase, Protein Expr. Purif. 10 (1997) 185–191.
[9] B.A. Beaupre, D.C. Forouzesh, G.R. Moran, Transient-state analysis of porcine dihydropyrimidine dehydrogenase reveals reductive activation by NADPH, Biochemistry 59 (2020) 2419–2431.
[10] D.C. Forouzesh, G.R. Moran, Mammalian dihydropyrimidine dehydrogenase, Arch. Biochem. Biophys. 714 (2021), 109066.
[11] D. Dobritzsch, G. Schneider, K.D. Schnackerz, Y. Lindqvist, Crystal structure of dihydropyrimidine dehydrogenase, a major determinant of the pharmacokinetics of the anti-cancer drug 5-fluorouracil, EMBO J. 20 (2001) 650–660.
[12] W.R. Hagen, M.A. Vanoni, K. Rosenbaum, K.D. Schnackerz, On the iron-sulfur clusters in the complex redox enzyme dihydropyrimidine dehydrogenase, Eur. J. Biochem. 267 (2000) 3640–3646.
[13] G.A. Ziegler, C. Vonrhein, I. Hanukoglu, G.E. Schulz, The structure of adrenodoxin reductase of mitochondrial P450 systems: electron transfer for steroid biosynthesis, J. Mol. Biol. 289 (1999) 981–990.
[14] P. Rowland, O. Bjornberg, F.S. Nielsen, K.F. Jensen, S. Larsen, The crystal structure of Lactococcus lactis dihydroorotate dehydrogenase A complexed with the enzyme reaction product throws light on its enzymatic function, Protein Sci. 7 (1998) 1269–1279.
[15] R.A.G. Reis, F.A. Calil, P.R. Feliciano, M.P. Pinheiro, M.C. Nonato, The dihydroorotate dehydrogenases: past and present, Arch. Biochem. Biophys. 632 (2017) 175–191.
[16] M. Bruschi, F. Guerlesquin, Structure, function and evolution of bacterial ferredoxins, FEMS Microbiol. Rev. 4 (1988) 155–175.
[17] B.A. Beaupre, D.C. Forouzesh, A. Butrin, D. Liu, G.R. Moran, Perturbing the movement of hydrogens to delineate and assign events in the reductive activation and turnover of porcine dihydropyrimidine dehydrogenase, Biochemistry 60 (2021) 1764–1775.
[18] D.C. Forouzesh, B.A. Beaupre, A. Butrin, Z. Wawrzak, D. Liu, G.R. Moran, The interaction of porcine dihydropyrimidine dehydrogenase with the chemotherapy sensitizer: 5-ethynyluracil, Biochemistry 60 (2021) 1120–1132.
[19] B.A. Beaupre, J.V. Roman, G.R. Moran, An improved method for the expression and purification of porcine dihydropyrimidine dehydrogenase, Protein Expr. Purif. 171 (2020), 105610.
[20] G.R. Moran, Anaerobic methods for the transient-state study of flavoproteins: the use of specialized glassware to define the concentration of dioxygen, Methods Enzymol. 620 (2019) 27–49.
[21] W. Holzerm, J. Shirdel, P. Zirak, A. Penzkoferm, P. Hegemann, R. Deutzmann, E. Hochmuth, Photo-induced degradation of some flavins in aqueous solution, Chem. Phys. 308 (2005) 69–78.
[22] R.N. Goyal, U.P. Singh, A.A. Abdullah, Electrochemical oxidation of uracil and 5-halouracils at pyrolytic graphite electrode, Indian J. Chem. 42 (2003) 42–47.
[23] M. Dulchavsky, C.T. Clark, J.C.A. Bardwell, F. Stull, A cytochrome c is the natural electron acceptor for nicotine oxidoreductase, Nat. Chem. Biol. 17 (2021) 344–350.
[24] R.L. Fagan, M.N. Nelson, P.M. Pagano, B.A. Palfey, Mechanism of flavin reduction in class 2 dihydroorotate dehydrogenases, Biochemistry 45 (2006) 14926–14932.
[25] R.L. Fagan, K.F. Jensen, O. Bjornberg, B.A. Palfey, Mechanism of flavin reduction in the class 1A dihydroorotate dehydrogenase from Lactococcus lactis, Biochemistry 46 (2007) 4028–4036.
[26] A.S. Abramovitz, V. Massey, Interaction of phenols with old yellow enzyme physical evidence for charge-transfer complexes, J. Biol. Chem. 251 (1976) 5327–5336.
[27] D.B. Longley, D.P. Harkin, P.G. Johnston, 5-fluorouracil: mechanisms of action and clinical strategies, Nat. Rev. Cancer 3 (2003) 330–338.
[28] G. Milano, M.C. Etienne, Dihydropyrimidine dehydrogenase (DPD) and clinical pharmacology of 5-fluorouracil (review), Anticancer Res. 14 (1994) 2295–2297.
[29] U. Amstutz, T.K. Froehlich, C.R. Largiader, Dihydropyrimidine dehydrogenase gene as a major predictor of severe 5-fluorouracil toxicity, Pharmacogenomics 12 (2011) 1321–1336.